# Random and channeling stopping powers and charge-state distributions in silicon for 0.2–1.2 MeV/u positive heavy ions

W. Jiang,* R. Grötzschel, W. Pilz, B. Schmidt, and W. Möller
*Research Center Rossendorf Inc., Institute of Ion Beam Physics and Materials Research, P.O. Box 510119, D-01314 Dresden, Germany*
(Received 3 April 1998)

Stopping powers and equilibrium charge-state distributions for 0.2–1.2 MeV/u $^{7}$Li, $^{11}$B, $^{12}$C, $^{14}$N, $^{16}$O, $^{31}$P, and $^{35}$Cl ions, measured in transmission of a 780 nm crystalline silicon foil, are reported. Using a high-resolution electrostatic analyzer, ion energy loss was determined within ±3%. The thickness of the Si foil was measured independently by Rutherford backscattering and SEM with an uncertainty of about 3–4 %. The random and channeling stopping powers were estimated within approximately ±5%, fitted using an empirical expression, and compared with the TRIM95 database. Resulting differences between the fitted and the empirical stopping powers were in the range of 5–15%, depending on ion species and incident beam energy. The equilibrium charge fractions were determined within about ±4% for most cases. At small angles to the {110} plane, the energy-loss spectra exhibit a multiple peak structure, primarily due to trajectory selection. [S0163-1829(99)07001-0]

## I. INTRODUCTION

Although ion-solid interactions have been investigated for nearly a century,[1] there is a relative dearth of experimental stopping power data for MeV heavy ions. In contrast to heavy ions, stopping power data for H and He ions in virtually all elemental materials are widely published, and empirical stopping parameters have been tabulated[2] with satisfactory accuracy. In addition, the precise stopping powers of H and He ions in amorphous silicon were recently determined and reported.[3] However, few experimental heavy-ion stopping power data are available for the refinement of current theoretical models of electronic energy loss and calculation of high-energy implant profiles. Heavy-ion stopping powers are also needed for analytical methods such as elastic recoil detection analysis and heavy-ion Rutherford backscattering spectrometry (HIRBS), where the accuracy of the stopping data directly affects the scale conversion from ion energy to target depth.

The situation is more critical for heavy ions incident on single crystals under axial or planar channeling conditions, for which cases accurate experimental stopping data are sparse. In addition, theoretical models that address energy loss for channeled particles are less well developed. For example, in the code crystal-TRIM,[4] stopping powers are normalized to the Ziegler, Biersack, and Littmark (ZBL) values.[5] To refine existing models for channeled heavy ions, accurate measurements of stopping powers seem to be necessary.

Charge-transfer processes also need to be studied in more detail. In a separate study,[6] frozen charge states were observed at energies above ~3 MeV/u for highly stripped, channeled ions incident on a ~1 $\mu$m thick Si crystalline foil. Also, charge-state equilibrium has been reported for 1.0–1.8 MeV nitrogen ions.[7] However, at ~1 MeV/u, detailed information (e.g., changes in the charge states of ions within channels) is still largely absent from the literature.

In this study, we present experimental stopping powers and equilibrium charge-state distributions of $^{7}$Li, $^{11}$B, $^{12}$C, $^{14}$N, $^{16}$O, $^{31}$P, and $^{35}$Cl ions in the energy range close to the stopping maximum (~1 MeV/u) in silicon for both random incidence and ⟨100⟩-axial and {110}-planar channeling directions. Trajectory-dependent energy-loss spectra for {110}-planar channeled ions are also reported.

## II. EXPERIMENTAL

The experimental setup, shown schematically in Fig. 1, was installed at the Rossendorf 5 MV tandem accelerator. The ion-beam collimation was effected by an adjustable cross slit (Slit 1) placed just behind the analyzing magnet, combined with a 200 $\mu$m diameter aperture located approximately 4.5 m downstream. The aperture was centered in the bottom of the 2 mm diameter Faraday cup (Cup 1) and thus allowed only ~1% of the beam to impinge on the target. No focusing elements were placed between the collimating optics. Because incident beam currents of only $\sim 10^{-12}$ A were required, the ion beams were defocused by means of a quadrupole lens located upstream from the switching magnet. A nearly homogenous intensity distribution over the entrance of Cup 1 resulted. The angular divergence of the ion beams was estimated at ~0.01°. A movable silicon detector (Det. 1) was positioned at a forward angle in the target chamber.

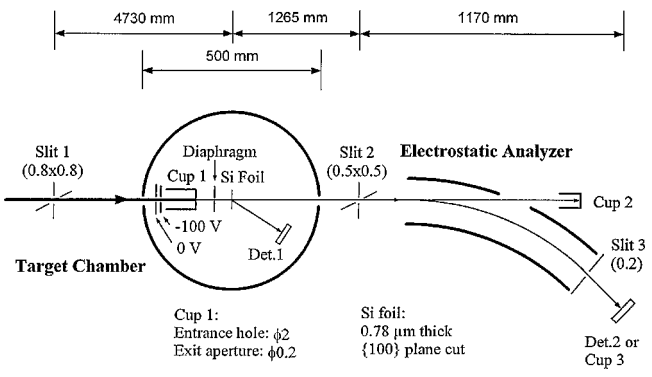


FIG. 1. Experimental arrangement.

 

TABLE I. Random and channeling stopping powers in crystalline silicon. Energy-loss measurement was made by an electrostatic analyzer in a transmission geometry with an acceptance angle of 0.03° in the beam direction. For most measurements the Si foil used was 0.78 $\mu$m thick, as determined by 1.5 MeV He RBS and SEM. Relative error of the experimental stopping data is about 5%.

| | | Random (MeV/$\mu$m) | | ⟨100⟩ axis (MeV/$\mu$m) | | | {110} plane (MeV/$\mu$m) | | |
|---|---|---|---|---|---|---|---|---|---|
| Ion | Energy (MeV) | Experiment | TRIM95 | Mean | Most probable | Least | Mean | Most probable | Least |
| $^{7}$Li | 1.8 | 0.51 | 0.52 | 0.47 | 0.47 | 0.42 | 0.45 | 0.45 | 0.40 |
| | 2.3 | 0.50 | 0.52 | 0.44 | 0.43 | 0.40 | 0.43 | 0.42 | 0.39 |
| | 2.8 | 0.48 | 0.51 | 0.39 | 0.39 | 0.35 | 0.40 | 0.39 | 0.36 |
| | 3.3 | 0.46 | 0.49 | 0.37 | 0.36 | 0.32 | 0.37 | 0.37 | 0.33 |
| | 3.8 | 0.46 | 0.47 | 0.35 | 0.35 | 0.31 | 0.36 | 0.35 | 0.32 |
| | 4.3 | 0.43 | 0.46 | 0.33 | 0.32 | 0.28 | 0.34 | 0.33 | 0.29 |
| | 4.8 | 0.42 | 0.44 | 0.30 | 0.29 | 0.26 | 0.32 | 0.31 | 0.28 |
| | 5.3 | 0.40 | 0.42 | 0.29 | 0.28 | 0.25 | 0.31 | 0.29 | 0.25 |
| | 5.8 | 0.39 | 0.41 | 0.27 | 0.26 | 0.23 | 0.29 | 0.28 | 0.24 |
| | 6.3 | 0.38 | 0.40 | 0.26 | 0.25 | 0.22 | 0.27 | 0.26 | 0.23 |
| $^{11}$B | 3.7 | 0.83 | 0.98 | 0.75 | 0.73 | 0.63 | 0.73 | 0.67 | 0.63 |
| | 5.7 | 0.85 | 0.97 | 0.76 | 0.73 | 0.62 | 0.72 | 0.67 | 0.60 |
| | 7.7 | 0.81 | 0.94 | 0.70 | 0.68 | 0.57 | 0.69 | 0.67 | 0.57 |
| | 9.7 | | 0.88 | 0.63 | 0.60 | 0.53 | 0.63 | 0.60 | 0.52 |
| | 11.7 | | 0.82 | 0.59 | 0.58 | 0.49 | 0.59 | 0.58 | 0.49 |
| $^{12}$C | 2.5 | 1.16 | 1.24 | 1.00 | 0.99 | 0.89 | 0.99 | 0.98 | 0.87 |
| | 4.5 | 1.17 | 1.24 | 0.96 | 0.94 | 0.79 | 0.99 | 0.98 | 0.83 |
| | 5.5 | 1.14 | 1.22 | 0.93 | 0.91 | 0.77 | 0.97 | 0.96 | 0.81 |
| | 7.5 | 1.11 | 1.20 | 0.91 | 0.91 | 0.73 | 0.93 | 0.93 | 0.78 |
| | 9.5 | 1.09 | 1.16 | 0.85 | 0.85 | 0.69 | 0.89 | 0.89 | 0.74 |
| | 11.6 | 1.06 | 1.11 | 0.79 | 0.78 | 0.64 | 0.82 | 0.81 | 0.69 |
| | 14.6 | 1.00 | 1.04 | 0.71 | 0.68 | 0.56 | 0.76 | 0.74 | 0.61 |
| | 19.6 | 0.95 | 0.91 | 0.62 | 0.56 | 0.46 | 0.70 | 0.64 | 0.53 |
| $^{14}$N | 4.5 | 1.36 | 1.50 | 1.15 | 1.12 | 0.94 | 1.15 | 1.15 | 0.98 |
| | 5.4 | 1.41 | 1.52 | 1.18 | 1.15 | 0.96 | 1.19 | 1.19 | 1.02 |
| | 6.5 | 1.40 | 1.54 | 1.16 | 1.13 | 0.95 | 1.17 | 1.17 | 1.00 |
| | 7.5 | 1.39 | 1.54 | 1.15 | 1.12 | 0.94 | 1.15 | 1.16 | 0.99 |
| | 8.5 | 1.40 | 1.53 | 1.16 | 1.14 | 0.95 | 1.17 | 1.18 | 1.00 |
| | 9.5 | 1.37 | 1.50 | 1.12 | 1.10 | 0.92 | 1.15 | 1.15 | 0.98 |
| | 10.5 | 1.34 | 1.47 | 1.08 | 1.06 | 0.87 | 1.10 | 1.13 | 0.86 |
| | 12.5 | 1.29 | 1.41 | 1.01 | 0.98 | 0.79 | 1.01 | 1.00 | 0.81 |
| | 14.5 | 1.27 | 1.36 | 0.96 | 0.95 | 0.75 | 0.97 | 0.94 | 0.78 |
| | 16.5 | 1.22 | 1.30 | 0.90 | 0.89 | 0.70 | 0.95 | 0.95 | 0.79 |
| | 19.5 | 1.18 | 1.23 | 0.82 | 0.83 | 0.63 | 0.90 | 0.91 | 0.76 |
| | 22.6 | 1.11 | 1.15 | 0.77 | 0.77 | 0.59 | 0.86 | 0.87 | 0.67 |
| | 25.5 | 1.09 | 1.10 | 0.73 | 0.72 | 0.57 | 0.81 | 0.75 | 0.57 |
| $^{16}$O | 5.3 | 1.59 | 1.70 | 1.38 | 1.37 | 1.24 | 1.39 | 1.37 | 1.26 |
| | 7.3 | 1.65 | 1.71 | 1.33 | 1.27 | 1.12 | 1.39 | 1.34 | 1.14 |
| | 9.3 | 1.64 | 1.70 | | | | | | |
| | 11.3 | 1.60 | 1.68 | 1.22 | 1.15 | 0.91 | 1.29 | 1.28 | 1.01 |
| | 14.4 | 1.56 | 1.64 | 1.13 | 1.08 | 0.85 | 1.21 | 1.13 | 0.90 |
| | 19.4 | 1.49 | 1.56 | 1.03 | 0.96 | 0.75 | 1.12 | 1.10 | 0.86 |
| $^{31}$P | 5.1 | 2.23 | 2.76 | 1.82 | 1.79 | 1.63 | 1.80 | 1.75 | 1.59 |
| | 7.9 | 2.61 | 3.05 | 2.37 | 2.31 | 2.06 | 2.24 | 2.15 | 2.00 |
| | 10.8 | 2.93 | 3.30 | 2.69 | 2.64 | 2.37 | 2.60 | 2.56 | 2.30 |
| | 13.8 | 3.10 | 3.56 | 2.92 | 2.84 | 2.56 | 2.82 | 2.75 | 2.50 |
| | 18.7 | 3.22 | 3.79 | 3.07 | 3.01 | 2.70 | 2.99 | 2.95 | 2.64 |
| $^{35}$Cl | 8.6 | 3.32 | 3.37 | 2.89 | 2.89 | 2.63 | 2.87 | 2.67 | 2.61 |
| | 18.4 | 3.78 | 4.14 | 3.42 | 3.44 | 3.05 | 3.32 | 3.34 | 2.94 |
| | 23.4 | 3.77 | 4.33 | 3.55 | 3.53 | 3.18 | 3.44 | 3.45 | 3.10 |
| | 28.4 | 3.89 | 4.38 | 3.68 | 3.65 | 3.27 | 3.55 | 3.50 | 3.12 |
| | 33.4 | 3.97 | 4.38 | 3.71 | 3.68 | 3.29 | 3.57 | 3.50 | 3.20 |

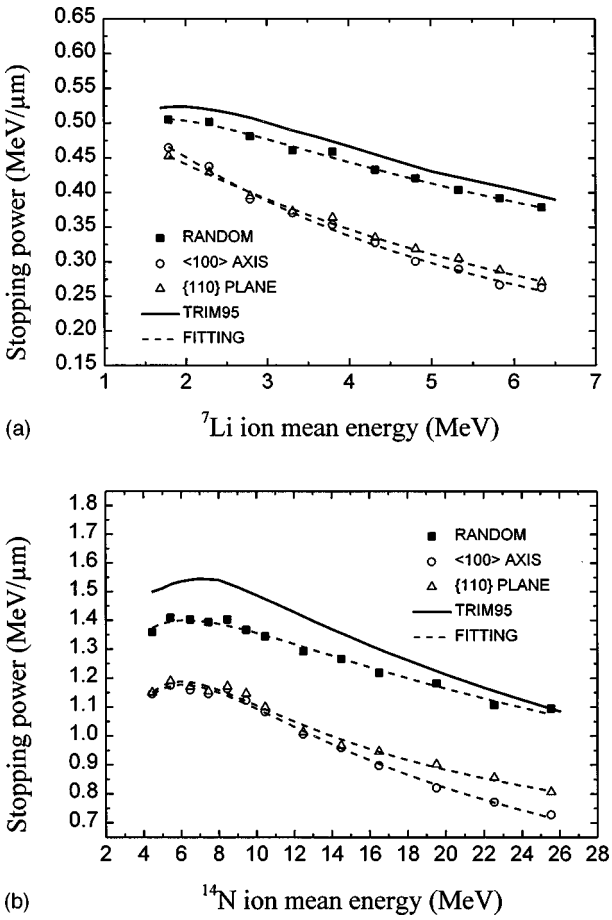


FIG. 2. Random and mean channeling stopping powers of (a) lithium ions and (b) nitrogen ions in crystalline silicon.

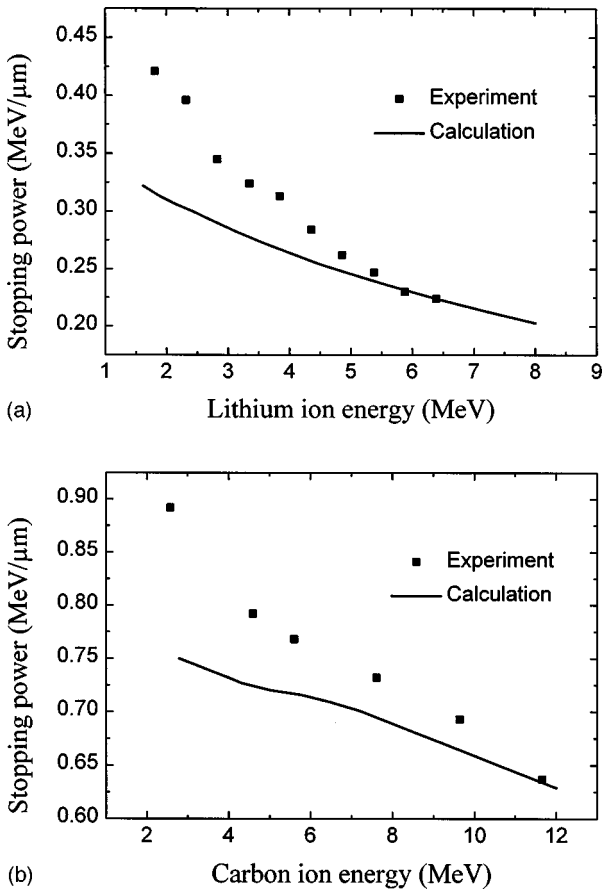


FIG. 3. Comparison of stopping powers of (a) lithium ions and (b) carbon ions best channeled in Si⟨100⟩ with semiempirical values from crystal-TRIM code.

Observation of the normalized yield on this detector provided an independent means of monitoring variations in beam intensity at Cup 1 during actual data acquisition.

Targets were mounted on a multiple sample holder attached to a precision goniometer. The goniometer provided two tilt axes perpendicular to the beam direction and was constructed from commercially available step-motor-driven rotational stages having a precision of ~0.05° on the horizontal axis and ~0.005° on the vertical axis. A linear translation stage integral with the goniometer was used to select separate spots on the target for study.

The charge states and energies of transmitted ions were analyzed by a Danfysik cylindrical electrostatic analyzer (ESA) with a mean radius of 2 m, a deflection angle of 30°, and a maximum bending power of 4 MeV/q at 40 kV. The acceptance angle of the ESA was limited to ~0.03° by a cross slit (Slit 2) placed at the entrance. Together with the 0.2 mm exit slit (Slit 3), this geometry provided an energy resolution power ($E/\delta E$) on the order of $\sim 10^3$. High voltage was exerted to the ESA by a bipolar power supply. Deflected particles were counted by a passivated implanted planar silicon detector (Det. 2). Direct beams were monitored by a retractable Faraday cup (Cup 3) for calibration of the ESA. The ESA was computer controlled via an optically coupled RS232 interface and an internal 16-bit DAC. All other functions of the experiment (e.g., data acquisition, crystal orientation, etc.) were implemented using CAMAC modules and our developed FORTRAN codes.

The vacuum pressure in the beamline, target chamber, and ESA was maintained below $2\times10^{-4}$ Pa. Under these conditions, the fraction of primary ions undergoing charge exchange with residual gases was less than $10^{-3}$.

## III. TARGET PREPARATION AND CHARACTERIZATION

Self-supporting single-crystal silicon foils of less than 1 $\mu$m thickness were prepared by standard electrochemical anisotropic etching[8] and subsequent isotropic etching. A thick Si wafer was anisotropically etched from the back in the absence of ambient light using a 30% $KOH/H_2O$ solution held at 80 °C. The resulting etch rate was ~70 $\mu$m/h. A patterned $SiO_2$ layer with window sizes of 1.2 mm×1.2 mm was used as a mask. Etching stopped when the wafer was reduced to a thickness of ~1.2 $\mu$m. Further thinning to less than 1 $\mu$m was effected by an isotropic etch performed at room temperature in a solution of $HF(\sim0.1\%)+H_2O+HNO_3$. A thin ⟨100⟩ Si foil prepared by this method was selected as the study sample throughout the experiments.

After transmission measurements the sample was analyzed by means of 1.5 MeV $He^+$ RBS using a ~70 $\mu$m diameter beam spot on the Rossendorf nuclear microprobe.[9] Although it was exposed to the heavy-ion beams for long periods, the sample showed no visible damage on three slightly overlapping study spots. The thickness and homogeneity of the sample were derived from the RBS spectra using published stopping data for He ions in Si, for which an ac-

TABLE II. Fitting parameters of stopping powers in crystalline silicon. Fitting formula (Ref. 3): $S(E) = E^{1/2} \ln(2.71828 + \beta E)/(\alpha_0 + \alpha_1 E^{1/4} + \alpha_2 E^{1/2} + \alpha_3 E + \alpha_4 E^{3/2})$, where ion energy $E$ is in MeV and stopping power $S(E)$ in MeV/$\mu$m. Mean stopping powers refer in channeling cases.

| Ion | $E$ (MeV) | Entrance | $\beta$ | $\alpha_0$ | $\alpha_1$ | $\alpha_2$ | $\alpha_3$ | $\alpha_4$ |
|---|---|---|---|---|---|---|---|---|
| $^{7}$Li | 1.8–6.3 | Random | 0.1960 | 1.6328 | −0.3389 | 0.2703 | 0.3041 | 0.3414 |
| | | ⟨100⟩ | −0.0022 | 0.9454 | −0.2932 | 0.5496 | 0.4180 | 0.3246 |
| | | {110} | −0.0374 | 0.7031 | −0.0917 | 0.7995 | 0.4052 | 0.2046 |
| $^{11}$B | 3.7–11.7 | Random | 0.8761 | 4.9573 | −1.7008 | −0.9195 | 0.5448 | 0.1846 |
| | | ⟨100⟩ | 0.2225 | 6.2336 | −2.4130 | −1.5587 | 0.6159 | 0.1536 |
| | | {100} | 0.7647 | 5.0061 | −1.7058 | −0.9265 | 0.5696 | 0.2225 |
| $^{12}$C | 2.5–19.6 | Random | 3.8528 | 0.1483 | −0.2895 | 1.2426 | 0.6175 | 0.0372 |
| | | ⟨100⟩ | 0.2402 | −2.4811 | 1.8740 | 2.1330 | −0.9418 | 0.2534 |
| | | {110} | 4.2590 | −0.3050 | 0.6058 | 1.4990 | 0.2341 | 0.1912 |
| $^{14}$N | 4.5–25.6 | Random | 5.4265 | 2.0650 | −0.7289 | 0.6511 | 0.4817 | 0.0563 |
| | | ⟨100⟩ | 2.3780 | 4.7515 | −1.4924 | −0.5251 | 0.4193 | 0.1532 |
| | | {110} | 0.1476 | 5.5031 | −2.7887 | −1.1765 | 0.7423 | −0.0046 |
| $^{16}$O | 5.3–19.4 | Random | 0.0338 | 3.3485 | −1.6010 | −0.6356 | 0.4618 | −0.0298 |
| | | ⟨100⟩ | 0.0230 | 1.5701 | −0.6082 | −0.1010 | 0.2376 | 0.0055 |
| | | {110} | 0.0489 | 2.7161 | −1.1682 | −0.4563 | 0.3689 | −0.0034 |
| $^{31}$P | 5.1–18.7 | Random | −0.0306 | 0.9529 | −0.0133 | −0.0023 | 0.0053 | 0.0002 |
| | | ⟨100⟩ | −0.0466 | 1.4629 | −0.0648 | −0.1006 | −0.0120 | 0.0024 |
| | | {110} | −0.0399 | 1.4532 | −0.0501 | −0.0896 | −0.0102 | 0.0026 |
| $^{35}$Cl | 8.6–33.4 | Random | 0.1186 | 1.0644 | −0.4414 | 0.0210 | 0.1060 | −0.0046 |
| | | ⟨100⟩ | 0.1726 | 1.1223 | −0.3554 | 0.0470 | 0.1053 | −0.0038 |
| | | {110} | 0.1766 | 0.9900 | −0.3188 | 0.0727 | 0.1065 | −0.0038 |

curacy of ±1% has been reported.[3] It was found that the average thickness of the sample was 780 nm with a uniformity of ~3% at the central point of analysis, i.e. the point on the surface of the sample where the majority of transmission measurements were performed. Across the 1 mm×1 mm area surrounding the central point, the measured thickness varied by ~7%.

Carbon buildup was observed during the course of transmission experiments. The final area density at the central point was $\sim 4\times10^{17}$ atoms/cm$^2$, corresponding to a 40 nm-thick amorphous carbon layer on both front and rear surfaces of the sample. At other spots on the sample, the carbon contamination was found to be lower. In all cases, the contribution of the carbon layers to ion stopping was taken into account in the data analysis.

Subsequent to $He^+$ RBS measurements, the thickness of the sample was confirmed by scanning electron microscopic (SEM) examination of a cross section through the central point. The average thickness was 800±50 nm, which is in good agreement with the RBS measurements.

## IV. RESULTS AND DISCUSSION

### A. Attainment of charge-state equilibrium

In the present study, 11 MeV nitrogen ions having charge states of $N^{2+}$, $N^{3+}$, and $N^{4+}$ were directed at the thin Si foil sample (~820 nm). RBS spectra were collected at fresh spots on the sample in both random and channeling geometry. As expected, the final random stopping powers and the emergent (transmitted) charge fractions did not change for different initial charge states.

As has been reported,[10] equilibrium thickness is on the order of $10^2$ Å for 1.0 MeV/u heavy ions in amorphous carbon. Hence, charge-state distribution was likely affected during transmission of the incident beam through the carbon layers on the surfaces of the sample. However, the contribution of the carbon layers to energy loss was small (~5%).

Assuming that particles are well channeled and charge states are frozen for all or most of the pathlength through the channel, fine structure or widely overlapping energy-loss peaks for each emergent charge state would be expected. This is because higher charge states result in larger stopping powers.[6] However, in this experiment, we did not observe such spectra. In addition, there was no evidence of any dependence of stopping power along ⟨100⟩ or {110} on the initial and final charge states. The charge-state fractions of emergent ions also coincided for different incident charge states. The results imply that the charge state frequently fluctuates inside the channel, as it does in the random case. As a result, 11 MeV N ions penetrating the silicon foil would be expected to reach charge state equilibrium under both random and channeling conditions. In addition, all other ion species investigated in this study ($3<Z_1<17$) exhibited the same behavior. That is, in the energy region of 0.2–1.2 MeV/u, stopping powers in Si were charge independent, and emergent charge fractions were nearly identical for the same outgoing energy. Therefore, the attainment of charge-state equilibrium was assumed in this study.

### B. Determination of heavy-ion stopping powers

Random stopping powers for each ion species were obtained from the energy peaks in the transmission spectra. A

TABLE III. Equilibrium charge-state distributions of $^{7}$Li, $^{11}$B, $^{12}$C, and $^{14}$N ions. Charge fraction measurement was made by an electrostatic analyzer in a transmission geometry. For most measurements the Si foil used was 0.78 $\mu$m thick, as determined by 1.5 MeV He RBS and SEM. All data refer to random cases, unless otherwise indicated. Relative error of the experimental charge fractions is about 4%.

| Energy (MeV) | Charge state | | | Energy (MeV) | Charge state | | | | | | |
|---|---|---|---|---|---|---|---|---|---|---|---|
| | $1^+$ | $2^+$ | $3^+$ | | $1^+$ | $2^+$ | $3^+$ | $4^+$ | $5^+$ | $6^+$ | $7^+$ |
| | $^{7}$Li | | | | | | | $^{11}$B | | | |
| 1.59 | 23.7 | 54.9 | 21.4 | 3.35 | 0.78 | 17.1 | 59.3 | 21.6 | 1.24 | | |
| 2.09 | 12.0 | 46.0 | 42.1 | 5.33 | | 6.2 | 47.9 | 41.2 | 4.7 | | |
| 2.59 | | 44.2 | 55.8 | 7.36 | | | 36.0 | 49.2 | 14.8 | | |
| 3.12 | | 38.6 | 61.4 | 9.36 | | | 21.4 | 53.4 | 25.2 | | |
| 3.60 | | 34.2 | 65.8 | | | | | | | | |
| 4.14 | | 28.6 | 71.4 | | | | | $^{12}$C | | | |
| 4.63 | | 22.7 | 77.3 | 2.05 | | 29.6 | 50.7 | 19.7 | | | |
| 5.17 | | 22.2 | 77.8 | 4.02 | | 3.98 | 32.1 | 55.6 | 8.35 | | |
| 5.67 | | 18.0 | 82.0 | 5.04 | | 1.84 | 21.6 | 59.9 | 15.9 | 0.80 | |
| 6.19 | | 17.8 | 82.2 | 7.06 | | | 10.0 | 57.3 | 30.0 | 2.69 | |
| | | | | 9.09 | | | 5.22 | 47.6 | 41.0 | 6.22 | |
| | $^{7}$Li⟨100⟩ | | | 11.1 | | | | 38.2 | 49.2 | 12.6 | |
| 1.62 | 18.3 | 55.7 | 26.0 | | | | | | | | |
| 2.14 | 10.1 | 48.6 | 41.3 | | | | | $^{14}$N | | | |
| 2.66 | 5.89 | 40.4 | 53.7 | 1.07 | 22.5 | 42.5 | 30.2 | 4.83 | | | |
| 3.19 | | 38.5 | 61.5 | 1.43 | 12.6 | 35.5 | 43.3 | 8.58 | | | |
| 3.69 | | 32.7 | 67.3 | 1.77 | 4.69 | 24.8 | 49.5 | 18.4 | 2.57 | | |
| 4.23 | | 28.7 | 71.3 | 2.26 | | 15.6 | 45.9 | 32.9 | 5.61 | | |
| 4.73 | | 25.2 | 74.8 | 2.97 | | 6.54 | 33.7 | 47.4 | 12.4 | | |
| 5.26 | | 21.1 | 78.9 | 3.90 | | | 20.6 | 53.2 | 25.1 | 1.12 | |
| 5.77 | | 19.5 | 80.5 | 4.10 | | 1.81 | 17.3 | 52.2 | 26.9 | 1.82 | |
| 6.28 | | 15.2 | 84.8 | 4.85 | | 1.18 | 12.1 | 47.2 | 36.2 | 3.31 | |
| | | | | 5.02 | | | 8.63 | 44.2 | 43.8 | 3.40 | |
| | $^{7}$Li{110} | | | 5.97 | | | 6.60 | 37.3 | 50.0 | 5.82 | 0.28 |
| 1.63 | 16.5 | 56.3 | 27.2 | 6.06 | | | 4.97 | 34.7 | 52.5 | 7.86 | |
| 2.14 | 10.5 | 47.0 | 42.5 | 6.89 | | | 4.94 | 30.4 | 55.3 | 8.69 | 0.71 |
| 2.66 | 5.57 | 41.9 | 52.5 | 7.91 | | | 2.73 | 23.4 | 58.2 | 15.1 | 0.56 |
| 3.19 | | 36.6 | 63.4 | 8.02 | | | 2.00 | 21.5 | 57.8 | 17.6 | 1.17 |
| 3.68 | | 30.5 | 69.5 | 8.89 | | | 1.72 | 20.8 | 59.2 | 17.0 | 1.25 |
| 4.22 | | 27.3 | 72.7 | 9.92 | | | 1.15 | 16.4 | 58.7 | 21.8 | 1.91 |
| 4.71 | | 23.7 | 76.3 | 10.1 | | | | 13.1 | 56.7 | 27.3 | 2.60 |
| 5.25 | | 22.6 | 77.4 | 12.0 | | | | 10.1 | 50.4 | 35.7 | 3.85 |
| 6.27 | | 16.5 | 83.5 | 14.0 | | | | 6.83 | 47.6 | 38.8 | 6.79 |

Gaussian model was used to determine the position of the peak maxima. Under channeling conditions, the energy-loss spectra were asymmetric, and mean stopping powers were defined by the average energy loss. The most probable stopping powers coincided with the transmission peak maxima. The least stopping powers corresponded to the energy at half-maximum on the trailing edge (high-energy side) of the peak. In all cases, the stopping powers were weighted based on the corresponding equilibrium charge fractions. The ion energy $\overline{E}$ was taken as the mean energy of the incident and transmitted ions: $\overline{E}=(E_{\text{in}}+E_{\text{out}})/2$.

Experimental stopping powers for 0.2–1.2 MeV/u $^{7}$Li, $^{11}$B, $^{12}$C, $^{14}$N, $^{16}$O, $^{31}$P, and $^{35}$Cl ions in Si are presented in Table I. The stopping data for Li and N are illustrated in Fig. 2. The experimental random stopping data for Li shown in Fig. 2(a) are in good agreement with ZBL semiempirical stopping data obtained from TRIM95.[5] The difference between the experimental and calculated random stopping powers is within the estimated experimental error of $\pm 5\%$. No difference was observed between the mean channeling stopping powers for lithium ions along ⟨100⟩ and {110}. The separation of random and channeling branches increased from 10% at $\overline{E}=1.8$ MeV to 30% at $\overline{E}=6.3$ MeV. The data for 4.5–25.5 MeV nitrogen ions at random incidence are shown in Fig. 2(b) and exhibit a broad stopping maximum. In comparison, TRIM95 database overestimates stopping powers across 4.5–12.5 MeV by approximately 7%. In the range 19.5–25.5 MeV, the experimental and empirical random stopping powers are consistent. The mean stopping powers for nitrogen ions channeled along ⟨100⟩ and {110} are essen-

TABLE IV. Equilibrium charge-state distributions of $^{16}O$, $^{31}P$, and $^{35}Cl$ ions. Charge fraction measurement was made by an electrostatic analyzer in a transmission geometry. For most measurements the Si foil used was 0.78 $\mu$m thick, as determined by 1.5 MeV He RBS and SEM. All data refer to random cases, unless otherwise indicated. Relative error of the experimental charge fractions is about 4%.

| Energy (MeV) | Charge state $2^+$ | $3^+$ | $4^+$ | $5^+$ | $6^+$ | $7^+$ | $8^+$ | $9^+$ | $10^+$ | $11^+$ | $12^+$ | $13^+$ | $14^+$ |
|---|---|---|---|---|---|---|---|---|---|---|---|---|---|
| | | | | $^{16}O$ | | | | | | | | | |
| 4.66 | 0.73 | 10.4 | 31.5 | 44.8 | 11.6 | 0.97 | | | | | | | |
| 5.56 | | 3.84 | 25.5 | 46.9 | 22.1 | 1.60 | | | | | | | |
| 6.61 | | 2.13 | 17.8 | 48.6 | 29.0 | 2.37 | | | | | | | |
| 8.62 | | 0.92 | 8.95 | 38.2 | 45.2 | 6.37 | 0.41 | | | | | | |
| 10.7 | | | 5.30 | 30.8 | 51.9 | 11.5 | 0.56 | | | | | | |
| 13.6 | | | 2.74 | 20.2 | 55.1 | 20.1 | 1.83 | | | | | | |
| 18.8 | | | | 11.4 | 50.5 | 32.4 | 5.73 | | | | | | |
| | | | | | | $^{31}P$ | | | | | | | |
| 4.12 | 0.34 | 1.48 | 8.45 | 28.5 | 37.8 | 18.3 | 3.46 | 1.69 | | | | | |
| 6.80 | | 0.19 | 1.65 | 11.2 | 30.2 | 34.6 | 17.7 | 4.13 | 0.30 | | | | |
| 9.68 | | | | 3.19 | 16.3 | 34.9 | 29.0 | 13.9 | 2.54 | 0.20 | | | |
| 12.5 | | | | 1.26 | 7.99 | 24.7 | 35.7 | 23.0 | 6.55 | 0.79 | 0.02 | | |
| 17.4 | | | | | 2.45 | 11.2 | 30.6 | 33.8 | 18.0 | 3.68 | 0.27 | | |
| | | | | | | | | $^{35}Cl$ | | | | | |
| 7.26 | | | 1.14 | 6.90 | 19.5 | 35.3 | 26.3 | 9.30 | 1.58 | | | | |
| 12.0 | | | | 0.90 | 5.21 | 19.0 | 33.0 | 28.0 | 11.3 | 2.29 | 0.34 | | |
| 16.9 | | | | | 1.08 | 7.14 | 20.1 | 32.9 | 26.6 | 9.78 | 2.29 | 0.14 | |
| 21.9 | | | | | | 2.46 | 12.2 | 27.0 | 30.4 | 19.56 | 7.54 | 0.87 | |
| 26.8 | | | | | | | 5.66 | 18.3 | 31.8 | 29.1 | 12.5 | 2.41 | 0.18 |
| 31.7 | | | | | | | | 12.0 | 27.9 | 33.7 | 20.1 | 5.68 | 0.67 |

tially identical up to 16 MeV. Across 19.5–25.5 MeV, approximately 10% greater stopping was observed for the {110} planar-channeled particles.

The small acceptance angle ($\sim$0.03°) of the electrostatic analyzer used in this study limited the observation of transmitted particles. In a TRIM95 simulation of a 780 nm-thick silicon target at random incidence, only 1% of 5 MeV nitrogen ions are transmitted within this acceptance angle, while 96% particles are deflected into a 2° cone. A complementary simulation using crystal-TRIM (Ref. 4) was also performed to obtain an estimate of the difference between the mean energy of particles transmitted through 0.03° and the mean energy of particles transmitted at all other possible scattering angles. This calculation was based on 5 MeV nitrogen ions transmitted through a 780 nm silicon target. At random incidence, the calculated variation in ion energy across 2° was $\sim$5 keV, and the total energy loss through the foil was $\sim$1100 keV. Compared to ions emerging in all other directions, particles recorded by the electrostatic analyzer experienced a mean energy loss only $\sim$0.1% less. In addition, nuclear stopping power is 2–3 orders less in magnitude than the electronic stopping power in the investigated energy range. Therefore, substantial corrections for the acceptance angle in the random stopping powers were not needed. This conclusion was also supported by Eisen *et al.*,[11] who found that the energy spectra for energetic helium ions in random transmission geometry were insensitive to variations of entrance slit dimensions (up to a factor of 4 in diameter) using a small acceptance solid angle ($8\times10^{-7}$ steradians). For 5 MeV protons penetrating a copper foil with a thickness of 2.60 mg/cm$^2$, Ishiwari *et al.*[12] observed an increase in the energy loss of about 1.4% at the emergence angle of 3.82°. This angular range contains a vast majority of scattering ions and the energy dispersion is well within our experimental error (5%) of the stopping powers. In contrast to random incidence, a crystal-TRIM simulation of 5 MeV nitrogen ions channeled along $\langle 100\rangle$ in a 780 nm Si target showed an 8% decrease in the mean energy loss across 0.02° compared with the 0.2° region containing 88% of the transmitted particles.

### C. Empirical fitting of stopping data

The random and mean channeling stopping powers presented in this study were fitted using the following empirical expression[3]

$$S(E)=\frac{E^{1/2}\ln(2.71828+\beta E)}{\alpha_0+\alpha_1E^{1/4}+\alpha_2E^{1/2}+\alpha_3E+\alpha_4E^{3/2}}, \qquad (1)$$

where $\beta$, $\alpha_0$, $\alpha_1$, $\alpha_2$, $\alpha_3$, and $\alpha_4$ are fitting parameters, and $E$ is the ion energy. The results of fitting the experimental data using this expression are presented in Table II, where stopping powers $S$ are given in units of MeV/$\mu$m and energy $E$ in MeV. The range of ion energies across which the fitting parameters are applicable is also listed in Table II. The experimental data for both random incidence and channeling closely fit this expression.

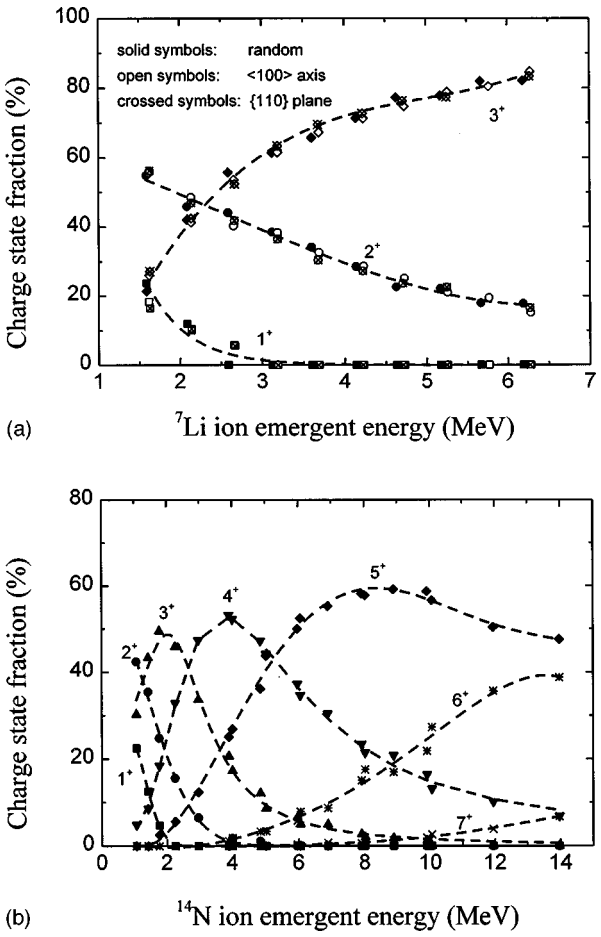


FIG. 4. Equilibrium charge state distributions of (a) lithium ions and (b) nitrogen ions in different target orientations. Dashed lines are just to guide the eye.

### D. Comparison with crystal-TRIM calculations

In crystal-TRIM,[4] binary collisions are assumed and the local inelastic energy loss of an ion is based on the Oen-Robinson model[13]

$$\Delta E_{\mathrm{el}} = S_{\mathrm{el}}^{\mathrm{ZBL}}(E)\,\frac{\exp[-C_{\mathrm{el}}\cdot 0.3\cdot(R_0(E,p)/a)]}{\int_0^{p_{\max}} 2\pi\,\exp[-C_{\mathrm{el}}\cdot 0.3\cdot(R_0(E,p)/a)]p\,dp}, \tag{2}$$

where $S_{\mathrm{el}}^{\mathrm{ZBL}}(E)$ denotes the ZBL electronic stopping power,[5] $R_0(E,p)$ the distance of closest approach, and $p_{\max}$ is the maximum impact parameter. The dimensionless quantity $C_{\mathrm{el}}$ is an empirical parameter close to unity, and $a$ is the universal screening length defined by

$$a=\frac{0.8854a_0}{Z_1^{0.23}+Z_2^{0.23}}. \tag{3}$$

For ions incident on a silicon crystal along the ⟨100⟩ axis, the least electronic stopping power can be estimated from the equation

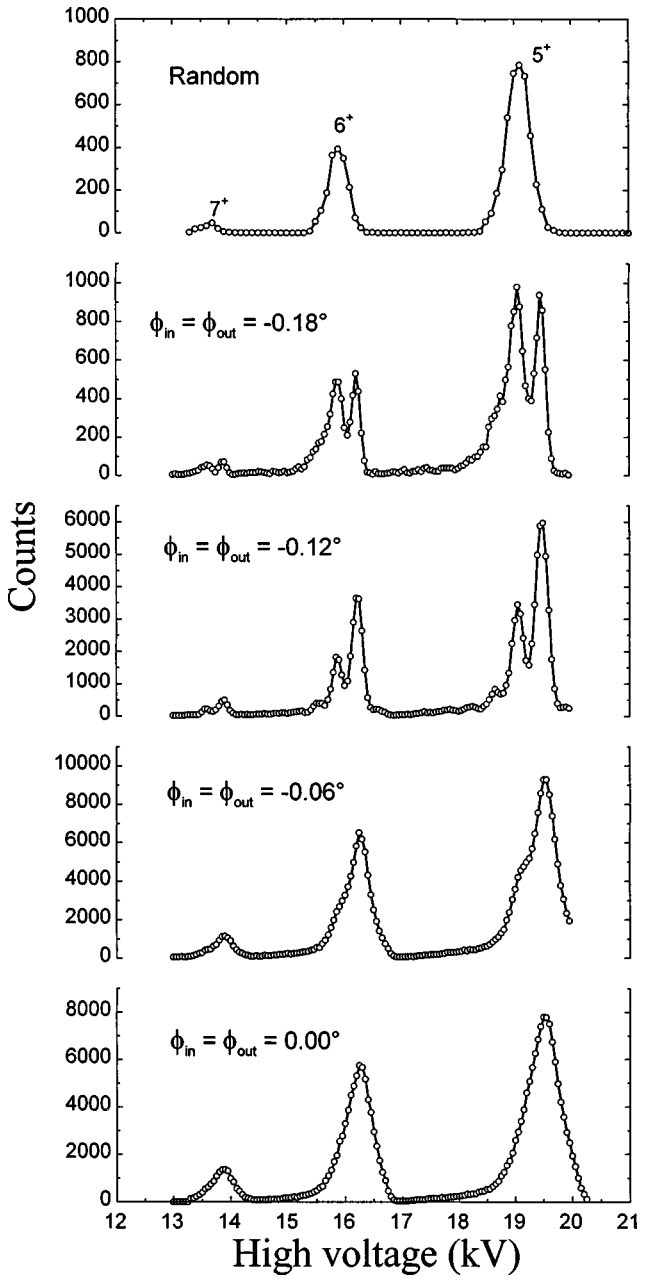


FIG. 5. ESA spectra of 11 MeV N ions penetrating 0.82 $\mu$m thick Si single crystal in different incident directions.

$$S(E)=\frac{\Delta E_{\mathrm{el}}(E,p)}{d_{\langle 100\rangle}}, \tag{4}$$

where the atomic spacing along the ⟨100⟩-axial string $d_{\langle 100\rangle}=d/4$, and $R_0(E,p)\approx p_{\max}=d/4$. The lattice constant $d$ for silicon is 0.543 06 nm. In the crystal-TRIM calculations, $C_{\mathrm{el}}$ in Eq. (2) was set to unity.

The results of the crystal-TRIM calculations for lithium and carbon ions are plotted together with the experimental data in Fig. 3. At higher energies, the calculated data (solid line) approach agreement with the experimental data (symbols), but discrepancies increase at lower energies.

For boron and chlorine, the crystal-TRIM calculations resulted in consistently smaller stopping powers than were obtained from the experimental data: for 4–8 MeV boron, the differences were 7–10%; for 10–35 MeV chlorine, differ-

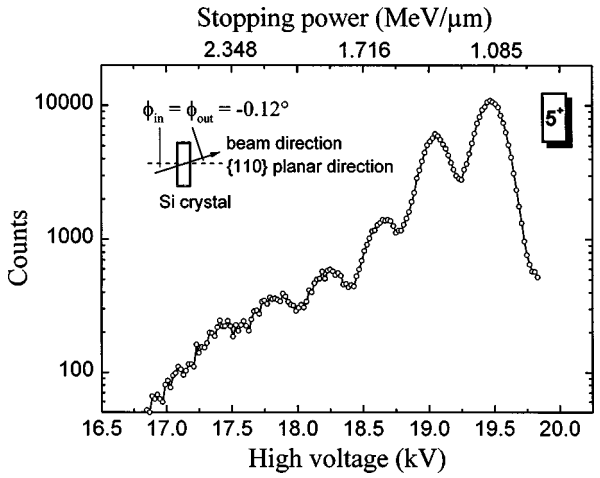


FIG. 6. Logarithmic plot showing fine structures of emergent charge state $5^+$ in Fig. 5.

ences of ~30% were observed. However, it should be noted that better agreement might have been obtained by fitting the parameter $C_{el}$ for this energy range.

### E. Equilibrium charge-state distribution

The experimental equilibrium charge-state distributions for 0.2–1.2 MeV/u $^{7}$Li, $^{11}$B, $^{12}$C, $^{14}$N, $^{16}$O, $^{31}$P, and $^{35}$Cl ions are given in Tables III. and IV. The fractions of lithium and nitrogen ions in all possible charge states are shown as a function of emergent energy in Fig. 4. Figure 4(a) illustrates that, in the case of Li, target orientation had virtually no impact on the transmitted charge fractions. Similarly, the data for nitrogen under random and channeling conditions were also on the same curve and are therefore plotted without symbol distinctions in Fig. 4(b).

It should be noted that contaminants, specifically the carbon layer that formed on the rear surface of the study sample, could influence or even determine emergent charge state. For example, in a related study of equilibrium charge-state distributions using various foils, mean charge values varied with the atomic number of the target.[14] However, that work also showed that 23.5 and 38.5 MeV chlorine ions emerging from silicon have a mean charge value within 2% of their mean charge upon emerging from carbon. At the energies used in the present study, the absolute difference of emergent charge from carbon and silicon targets is even smaller. Therefore, the carbon contamination on the sample had little effect on equilibrium charge-state distribution.

### F. Trajectory dependence of energy-loss spectra

The small acceptance angle of the electrostatic analyzer was aligned in the direction of the beam, so that the incident angle ($\phi_{in}$) was equal to the emergent angle ($\phi_{out}$). This condition allowed the observation of ions channeled along certain specific trajectories[15] because only ions, which had been deflected within this small angle, could be detected.

Figure 5 shows the energy loss spectra of 11 MeV nitrogen ions penetrating the silicon sample. The energy-loss spectra of the $5^+$, $6^+$, and $7^+$ emergent charge states are plotted for random incidence, at small angles to {110}, and in {110}-planar channeling. In the random spectrum, the charge-state peaks are well resolved and have similar, Gaussian-type distributions, but the peaks exhibit different intensities. As the angle of incidence approaches the {110} planar direction, group structure appears in the charge-state peaks. The fine structure peak intensities also change rapidly with tilt. At $-0.18°$, two branches of nearly equal intensity but different energy loss are evident for each emergent charge state. At $-0.12°$, more fine structure peaks appear, but the energies at the fine peaks are unchanged relative to those at $-0.18°$. The fine structure of the $5^+$ charge state at $-0.12°$ incidence is shown in detail in a logarithmic plot (Fig. 6), which shows at least five fine-structure peaks. Similar fine structure has been observed for 4 MeV lithium ions.[16] Returning to Fig. 5, only poorly resolved fine structure is seen at $-0.6°$, but the principal fine peak energy remains the same as at $-0.12°$ and $-0.18°$. In {110}-planar channeling, only a single peak appears for each charge state. The charge-state peaks in the channeling spectrum are asymmetric and show long tails on the low-energy side of the maxima.

## V. SUMMARY

Charge-state equilibrium was attained in charge exchange processes for 0.2–1.2 MeV/u lithium through chlorine ions penetrating a 780 nm silicon foil in random incidence, ⟨100⟩-axial and {110}-planar channeling directions. The electronic stopping powers of 0.2–1.2 MeV/u $^{7}$Li, $^{11}$B, $^{12}$C, $^{14}$N, $^{16}$O, $^{31}$P, and $^{35}$Cl ions in silicon were measured and fitted. Comparisons of the experimental stopping powers with empirical values from TRIM95 and crystal-TRIM showed the predicted stopping powers were systematically larger for random incidence, but generally smaller for channeled particles. Equilibrium charge-state distributions of the emergent ions across the energy range studied were also determined. The trajectory-dependent energy-loss distributions of 11 MeV N ions and 4 MeV Li ions through a silicon target showed distinct fine structure at small angles to the {110} plane.

## ACKNOWLEDGMENTS

We would like to thank D. Grambole and F. Herrmann for their microprobe RBS characterization of the silicon sample, and R. Müller for her complementary SEM analysis. We also thank M. Posselt for his thoughtful advice and helpful assistance in using crystal-TRIM. The skillful operation team of the Rossendorf tandem accelerator is also gratefully acknowledged for providing the high-quality beams used for this experiment. Lastly, W. Jiang thanks D. E. McCready of the Pacific Northwest National Laboratory in Richland, Washington, USA for his careful editing of the manuscript.

*Author to whom correspondence should be addressed: Pacific Northwest National Laboratory, P.O. Box 999, MSIN K8-93, Richland, WA 99352, USA, Fax +1 509 376 5106. Electronic address: Weilin.Jiang@pnl.gov

[1] N. Bohr, Philos. Mag. **25**, 10 (1913).

[2] H. H. Andersen and J. F. Ziegler, *Hydrogen Stopping Powers and Ranges in All Elements* (Pergamon, New York, 1977); J. F. Ziegler, *Helium Stopping Powers and Ranges in All Elements* (Pergamon, New York, 1977).

[3] D. Niemann, P. Oberschachtsiek, S. Kalbitzer, and H. P. Zeindl, Nucl. Instrum. Methods Phys. Res. B **80/81**, 37 (1993); D. Niemann, G. Konac, and S. Kalbitzer, *ibid.* **118**, 11 (1996).

[4] M. Posselt, Radiat. Eff. Defects Solids **130/131**, 87 (1994).

[5] J. F. Ziegler, J. P. Biersack, and U. Littmark, *The Stopping and Range of Ions in Solids* (Pergamon, New York, 1985), Vol. 1.

[6] J. P. Biersack, Nucl. Instrum. Methods Phys. Res. B **80/81**, 12 (1993); J. A. Golovchenko, A. N. Goland, J. S. Rosner, C. E. Thorn, H. E. Wegner, H. Knudsen, and C. D. Moak, Phys. Rev. B **23**, 957 (1981).

[7] G. G. Bentini, M. Bianconi, and R. Nipoti, Nucl. Instrum. Methods Phys. Res. B **80/81**, 33 (1993).

[8] B. Schmidt, J. von Borany, U. Todt, and A. Erlebach, Sens. Actuators A **41/42**, 689 (1994).

[9] D. Grambole, F. Herrmann, and B. Herrmann, Nucl. Instrum. Methods Phys. Res. B **109/110**, 667 (1996); F. Herrmann and D. Grambole, *ibid.* **104**, 26 (1995).

[10] V. P. Zaikov, E. A. Kral'kina, N. F. Vorobjev, I. S. Dmitriev, V. S. Nikolaev, and Y. A. Teplova, Nucl. Instrum. Methods Phys. Res. B **5**, 10 (1984).

[11] F. H. Eisen, G. J. Clark, J. Bøttiger, and J. M. Poate, Radiat. Eff. **13**, 93 (1972).

[12] R. Ishiwari, N. Shiomi-Tsuda, N. Sakamoto, and H. Ogawa, Nucl. Instrum. Methods Phys. Res. B **51**, 209 (1990).

[13] O. S. Oen and M. T. Robinson, Nucl. Instrum. Methods **132**, 647 (1976).

[14] K. Shima, Nucl. Instrum. Methods Phys. Res. B **10/11**, 45 (1985).

[15] S. Datz, C. D. Moak, T. S. Noggle, B. R. Appleton, and H. O. Lutz, Phys. Rev. **179**, 315 (1969).

[16] Jiang Weilin, Ph.D. thesis, TU Dresden, 1997.